Applied Energy 302 (2021) 117561

Contents lists available at ScienceDirect

Applied Energy

journal homepage: www.elsevier.com/locate/apenergy

Utilization of thermoelectric technology in converting waste heat into electrical power required by an impressed current cathodic protection system

Fatemeh Delfani [a], Nader Rahbar [b,*], Cyrus Aghanajafi [c], Ali Heydari [d], Abdollah KhalesiDoost [b]

[a] Department of Mechanical Engineering, Semnan Branch, Islamic Azad University, Semnan, Iran
[b] Energy and Sustainable Development Research Center, Semnan Branch, Islamic Azad University, Semnan, Iran
[c] Faculty of Mechanical Engineering, K. N. Toosi University of Technology, Tehran, Iran
[d] Department of Mechanical Engineering, University of Torbat Heydarieh, Torbat Heydarieh, Khorasan Razavi, Iran

HIGHLIGHTS

- Converting waste heat to electrical power using thermoelectric technology.
- The generated power was utilized in an impressed current cathodic protection system.
- Using mathematical modeling and Buckingham Pi theorem for performance evaluation.
- Proposing three models to evaluate the performance of the system.

ARTICLE INFO

Keywords:
Buckingham Pi Theorem
Corrosion protection
Dimensional analysis
Impressed current cathodic protection
Waste heat recovery
Thermoelectric module

ABSTRACT

Supplying an energy source for impressed current cathodic protection is considered as the main challenge for pipelines corrosion protection in remote areas. The purpose of this study is to construct and evaluate the performance of an impressed current cathodic protection system using waste heat to replace the external electrical power supply. The system consists of four thermoelectric modules producing the electrical power from the hot combusted gas stream. Mathematical modeling and Buckingham Pi theorem were applied to obtain five dimensionless parameters and several models to estimate the system performance. According to the experimental results, the generated voltage, electrical current, and temperature difference have been increased rapidly during the experiment up to 201 mV, 44 mA, and 20 K, respectively. Moreover, mathematical modeling and Buckingham Pi theorem were also utilized to obtain three equations, two nonlinear and one dimensionless equation, to calculate the generated electrical voltage with the maximum error of 1.22%, 9.11%, and 10%, respectively. The results indicate that the temperature difference (between inlet gas and environment) and the figure of merit have a direct effect, and heat sink thermal resistance has an inverse effect on the generated electrical voltage.

1. Introduction

Corrosion is a destructive electrochemical activity. It is one of the most severe problems in all underground and submarine metal structures. It also causes direct and indirect economic and ecological damage. Among the methods of corrosion protection, one of the most effective ones is the cathodic protection (CP) which is the cathodization of the structure with two techniques, the impressed current cathodic protection (ICCP) and the sacrificial anode cathodic protection (SACP) that ultimately prevents corrosion [1,2].

In the sacrificial anode cathodic protection method, a metal or an alloy of metal, being more reactive than a protected metal, is attached to the structure that oxidizes instead of the original structure. However, due to the uncertainty of the anodes' life, they must be monitored and replaced at regular intervals, which has made this method cost-ineffective. Additionally, for structures that need high protective current, this method has a limited output and does not have the appropriate efficiency [3].

In the impressed current cathodic protection method, due to the

* Corresponding author.
E-mail addresses: Rahbar@semnaniau.ac.ir (N. Rahbar), aghanajafi@kntu.ac.ir (C. Aghanajafi), a.heydary@torbath.ac.ir (A. Heydari).

https://doi.org/10.1016/j.apenergy.2021.117561
Received 24 April 2021; Received in revised form 31 July 2021; Accepted 5 August 2021
Available online 14 August 2021

Nomenclature

a	Accuracy
A	Area, m^2
C_p	Specific heat, $J.kg^{-1}.K^{-1}$
D	Diameter, m
D_h	Hydraulic diameter, m
E	Energy, j
g	Gravitational acceleration, $m.s^{-2}$
h	Heat transfer coefficient, $W.m^{-2}.K^{-1}$
I	Electrical current, A
K	Air thermal conductivity, $W.m^{-1}.K^{-1}$
$\dot{m}$	Mass flow rate, $kg.s^{-1}$
Nu	Nusselt number
Pr	Prandtl number
q	Heating transfer, W
R	Electrical resistance, Ω
Ra	Rayleigh number
T	Temperature, K
u	Uncertainty
V	Electrical voltage, V
W	Electrical power, W
Z	Thermoelectric figure of merit, K^{-1}

Greek symbols

α_m	Seebeck coefficient, $m^2.s^{-1}$
β	Volume expansion coefficient, K^{-1}
γ_m	Thermal conductivity of thermoelectric module, $W.K^{-1}$
ΔT	Temperature difference, K
ν	Kinematic viscosity, $m^2.s^{-1}$
ρ_m	Electrical resistance of thermoelectric module, Ω
σ	Stefan-Boltzmann constant, $W.m^{-2}K^{-4}$

Subscripts

a	Air
b	Box
c	Cold
con	Convective
h	Hot
in	Inlet
m	Mean
o	Outlet
p	Pipe
r	Radiation
t	Total
T	Thermoelectric

presence of an external electrical source, the lifespan is increased and it saves the cost of monitoring and replacement. It can also create high current for the proper protection of various structures [4]. However, due to the need for a fixed external power supply, this system faces several issues, such as the maintenance of power supply equipment. In most cases, access to the required electricity is not available or very difficult and expensive in remote areas [5].

Several research have been conducted to replace applying clean and renewable energy, including solar and wind, to supply the electricity needs for cathodic protection [6]. However, one of the disadvantages of these systems is the lack of solar energy at night and non-stable cathodic protection in case of using wind energy and their need for energy storage [7]. El-Shakour and Anis [8] employed a microprocessor in a photovoltaic cathodic protection system for automatic current control, which was compared with the new system with conventional cathodic protection systems because ordinary systems use manual method to control the flow. Therefore, they proposed a new system which the cost of adding a new system is less than the cost of saving in case of corrosion. Lastly, they explained the benefits of utilizing a microprocessor system, such as eliminating the cost of technicians traveling to remote areas, saving time and effort, and minimizing the risk of corrosion. Laoun et al. [9] used solar panels to generate the required ICCP cathodic protection current. They noticed that when the number of thermoelectric modules and batteries were 10 and 14, respectively. This design could effectively protect the pipeline in all kinds of lands and all kinds of pipe components. The output current was high enough, low-cost, varied, and controllable. Javadi et al. [10] designed a cathodic protection system through the use of an intelligent photovoltaic power system in order to protect underground pipelines. As a result, the dimensions, weight, and the cost of installing and building the system were significantly reduced. They also proposed and tested two new controllers for this system. The simulation results proved the correct operation of both controllers and the whole system despite the different amounts of solar radiation and radiation duration. Polder et al. [11] evaluated the maintenance and performance data of 100 structures in which cathodic protection was used for concrete structures in the Netherlands. They revealed that components corrosion is finite and a function of age and minor repairs are required after approximately 15 years. Gadala et al. [12] experimentally and numerically studied the effects of soil physicochemistry and aeration surface on the cathodic protection design in the underground pipeline. They reported that in places farther away from the CP anodes, corrosion increases in cold-dry soils. This is due to increased gas transfer, accelerated reaction rate, and the lack of cathodic protection. Additionally, in most areas with no large cover the corrosion rate decreased despite the CP currents. Moreover, as moisture was increased, soil conductivity was increased and the external surfaces were better protected via cathodic protection. Finally, by use of this model, the potentials and anode placements were determined, thus, the efficiency and overproduction of cathodic protection reached their maximum value. They stated that these studies comprise this feature in other geometries and environments. Hameed et al. [13] numerically modeled cathodic protection via ICCP method for steel pipes in saltwater. There was about a 1.27% error between modeling and laboratory data implying that this method is suitable for corrosion problems. They achieved high accuracy values for current density and potential. Sercio et al. [14] modeled the cathodic protection on a finite element method (FEM) steel impeller shaft. The items evaluated in their work were the effects of shaft rotation and seawater flow. They observed that very little polarization was experienced under various conditions, including fixed shafts, rotating shafts, and the absence of water renewal. Furthermore, when the water was not renewed, and the shaft was not moving, it was observed that the potential had reached less than the limits of European standards related to adequate cathodic protection.

Thermoelectric modules are devices used for converting temperature differences into electricity and vice versa. They are divided into thermoelectric coolers (TEC) and thermoelectric generators (TEG). These systems are highly reliable, modular, cheap, easy-to-control, small-sized, silent due to having no moving parts, environmentally friendly, pollution-free, and low-cost in maintenance [15]. According to these advantages, thermoelectric modules include a wide range of industrial applications, such as spacecraft [16], solar intensity measurement [17], solar desalination systems [18,19], fuel cells waste heat recovery [20], cooling [21], vehicle exhaust waste heat recovery [22], and atmospheric energy harvesting [23].

In regard to the thermoelectric ability to convert heat into electricity, thermoelectrics are applied in cathodic protection to supply the required

electrical energy. In an experimental study, Yezhovet et al. [24] utilized thermoelectric modules to generate electrical energy supplying the cathodic protection of the pipeline. They also proposed some equations for calculating the thermoelectric properties that could be used to adjust the flow characteristics according to the gas temperature and flow rate. Rahman [25] connected the thermoelectric generators to the ship's exhaust gas section to generate electricity for impressed current cathodic protection. He reported that force circulation provided a more stable and efficient current and voltage compared to natural circulation. Lishuet et al. [26] employed a thermoelectric module to convert the heat of underground heating pipelines into electrical energy used in the cathodic protection of greenhouse heating pipeline. The results indicated a temperature difference of 33.2 °C between the two sides of the thermoelectric and a 92.97% degree of protection confirming the usability and practicality of their research.

1.1. Motivation for conducting this research

As mentioned above, impressed current cathodic protection, one of the most effective methods of corrosion control, needs an electrical power supply. However, most structures that need corrosion protection are located in remote and inaccessible areas. Thus, supplying electricity to the ICCP is one of the most significant challenges for engineers. Therefore, renewable energy sources, such as solar and wind energies have been used in previous studies to solve the ICCP power supply problem. However, due to the lack of solar energy at night and non-stability in wind energy, these methods require energy storage which is costly and comprises several difficulties.

The question is how to provide a stable energy source for cathodic protection in remote areas. Using gas inside the pipeline could be a firm source for thermal energy production. Considering the mentioned advantages of thermoelectric technology and its ability to the energy conversion, this thermal energy could be converted into an electricity source required for cathodic protection. It eliminates the need for continuous maintenance of the system due to the lack of moving parts, and it can be used in remote areas with no access to the distribution network. To the best of our knowledge, there are a few studies on the use of thermoelectric technology in the cathodic protection systems. On the other hand, mathematical modeling of such devices has not been presented yet. This study aimed to construct a thermoelectric cathodic protection system and evaluate its behavior and performance under different conditions. In addition to the experimental method, mathematical modeling is also applied to evaluate the performance of the proposed system and three models will be presented to estimate the performance of the proposed systems.

2. Theoretical background

In this section, the basic principles utilized in the mathematical modeling of the proposed system are presented. These relations are divided into two categories, thermoelectric and heat transfer relations.

2.1. Heat transfer relations

Heat transfer can be divided into natural and forced convection. When a stream of hot gas passes through a pipe, the heat transfer from the gas stream to the wall is calculated from the following equations [27,28]:

$$q = \dot{m} C_p (T_{in} - T_o) \tag{1}$$

$$q = hA\left(T_m - T_p\right) \tag{2}$$

that $\dot{m}$, T_{in}, T_o, T_m, T_p, h, and A are gas mass flow rate, gas inlet temperature, gas outlet temperature, gas mean temperature, pipe temperature, convection heat transfer coefficient, and pipe surface area, respectively. For natural convective heat transfer inside a hollow pipe, the heat transfer coefficient is calculated by the following equations [27,29]:

$$Nu = \frac{hK}{D} = c \times Ra^n \tag{3}$$

$$Ra = \frac{g \times \beta \times \Delta T \times D^3 \times Pr}{\nu^2} \tag{4}$$

in the above equations, K, ν, D, and $\Delta T$are gas thermal conductivity, gas kinematic viscosity, pipe diameter, and temperature difference, respectively.

2.2. Thermoelectric relations

The thermoelectric generator's geometry is represented in Fig. 1. Due to the transferred heat from the hot side to the thermoelectric and the transferred heat from the cold side of the thermoelectric, a temperature difference occurs between the two sides of the thermoelectric module producing an electrical potential difference in the system. According to the following equations, the input and output heat of a thermoelectric is achieved [30]:

$$q_h = \alpha_m I T_h - \frac{1}{2}\rho_m I^2 + \gamma_m \Delta T \tag{5}$$

$$q_c = \alpha_m I T_c + \frac{1}{2}\rho_m I^2 + \gamma_m \Delta T \tag{6}$$

where

$$\Delta T = T_h - T_c \tag{7}$$

The output voltage produced by the temperature difference in the thermoelectric generator is obtained from the following equation [20]:

$$V = \alpha_m \Delta T - \rho_m I \tag{8}$$

The difference between the input and output heat is equal to the thermoelectric's generated power and it is calculated by the following equation:

$$W = q_h - q_c = \alpha_m I \Delta T - \rho_m I^2 \tag{9}$$

3. Experimental procedure

Fig. 2 demonstrates an exploded view of the experimental setup utilized in the current study. As shown in this figure, the setup consists of six main parts: burner, steel pipe and box, mineral wool insulation, four thermoelectric modules, and aluminum heat sinks. The warm combusted gas rises in the steel pipe due to the stack effect (natural convection effect) and heats the pipe and the box. To prevent heat loss, the pipe is covered with mineral wool insulation with a thickness of 0.04 m. Four thermoelectric modules were placed on the other side of the box. The output heat caused a temperature difference between the two sides of the thermoelectric modules, which produce an electric voltage in the system.

As previously mentioned, thermoelectric modules are divided into two types of thermoelectric generators (TEG) and thermoelectric coolers (TEC). For operating temperatures below 373 K, thermoelectric coolers perform better in generating electrical power [20]. Herein, four thermoelectric coolers (model TEC1-12706) were employed for generating the electrical power from the combusted gas stream. Moreover, four heat sinks were applied to cool down the thermoelectric generators and to make a temperature difference between the two sides of the thermoelectric modules. Each heat sink comprises 11 fins with a thickness of 0.002 m. The dimensions of the system components are displayed in Table 1. Table 2 presents the properties of the thermoelectric modules. The pictorial and schematic views of the setup during experimentation

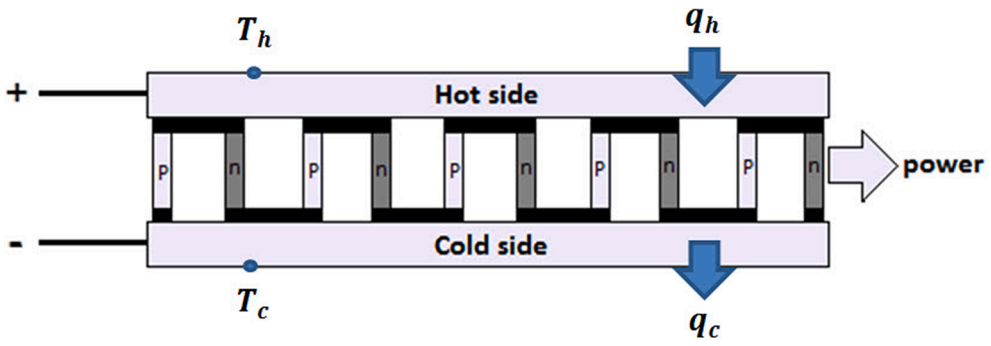

Fig. 1. The schematic view of a thermoelectric generator [17].

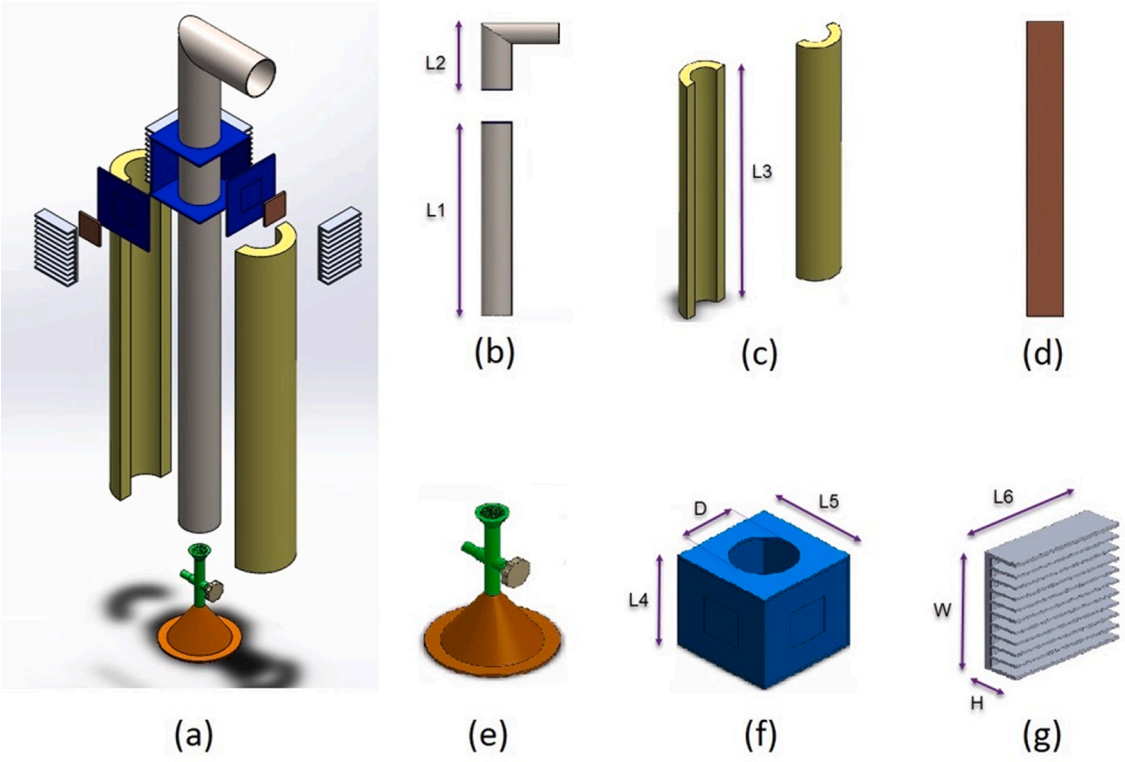

Fig. 2. (a) The exploded view of the experimental setup (b) pipe (c) insulation (d) thermoelectric (e) burner (f) box (g) heatsink.

Table 1
The dimensions of the system components.

Dimension	Size	Unit
L1	0.556	m
L2	0.189	m
L3	0.556	m
L4	0.100	m
L5	0.100	m
D	0.060	m
W	0.0908	m
L6	0.0652	m
H	0.0198	m

Table 2
The properties of the thermoelectric used in this research.

Properties	Related parameter	-	Unit
Thermoelectric model	–	TEC1-12706	–
Manufacturer	–	Thermonomic Inc.	–
Dimensions	A_T	0.04 × 0.04	m^2
Seebeck coefficient	α_m	0.0157	$V.K^{-1}$
Electrical resistance	ρ_m	2.2	Ω
Conductivity coefficient	γ_m	0.8436	$W.K^{-1}$

are shown in Figs. 3 and 4, respectively.

Experiments were performed on October 3, 2020, in a room with a controlled environment and the ambient temperature of 22°C. The values of electrical current and output voltage, thermoelectric hot and cold side temperatures, and pipe surface temperature were measured in different time intervals.

The uncertainty is usually expressed as an interval around the estimated value. There are two types of uncertainty: Type A and Type B. Type A is related to random errors and can be measured with statistical analysis. Type B is related to systematic errors and may be determined by looking up specific information about a measured data found in the calibration report or the data book of the measuring device [31,32]. In this research, the measuring devices (temperature sensors and multimeter), comprise continuous variables and there is no statistical

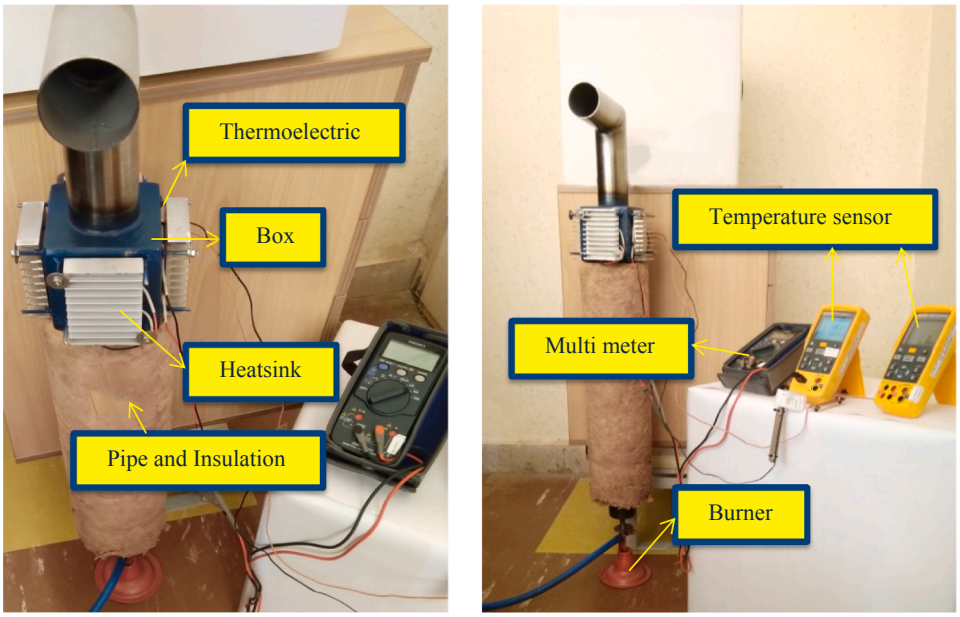

Fig. 3. The experimental setup's different view.

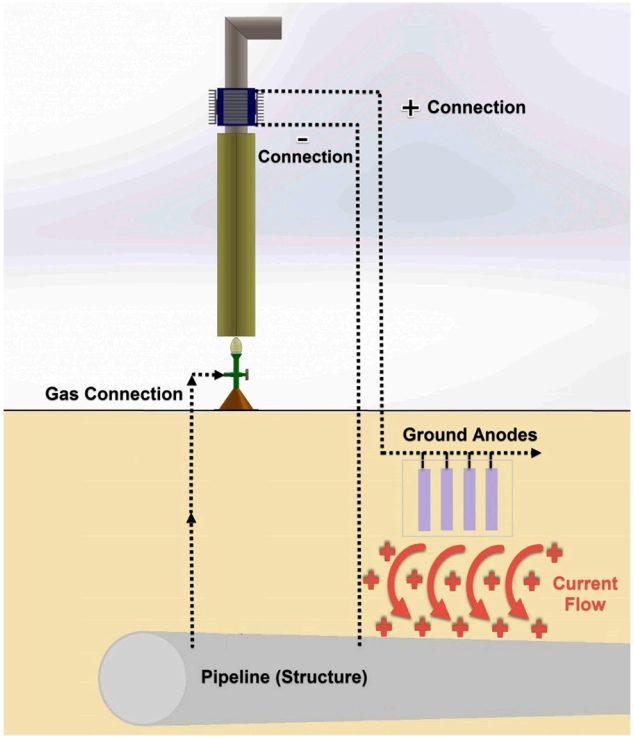

Fig. 4. The schematic view of the cathodic protection system in a real application.

analysis in the experimental procedure. Therefore, the uncertainties of their reading values are always Type B [33].

In this work, the uncertainties (Type B) are calculated from the following equation [34,35]:

$$u = \frac{a}{\sqrt{3}} \tag{10}$$

where a and u indicate the accuracy of the measuring device and the standard uncertainty, respectively. Table 3 represents the uncertainties related to the experimental facilities:

Table 3
The standard uncertainties associated with the measuring devices.

Measuring device	Accuracy	Range	Standard uncertainty
Temperature sensor (Type K)	0.1 $^{\circ}C$	0 –900 $^{\circ}C$	0.06 $^{\circ}C$
Multi meter (voltage)	0.1 V	0 –20 V	0.06 V
Multi meter (current)	0.1 A	0 –10 A	0.06 A

4. Mathematical modeling

The purpose of mathematical modeling of an engineering system is to formulate its behavior and to estimate its performance under different conditions. With mathematical modeling, the system performance can be predicted with appropriate accuracy, at a lower cost, and in a shorter time without having to build different types and performing various experiments on the systems [36,37]. The forementioned experimental setup consists of four parts; pipe, box, thermoelectric modules, and heat sinks. For performing the mathematical modeling, the energy balance equations are separately derived for each part, and finally the mathematical model of the system is obtained by combining these equations. Following assumptions have been considered to simplify the problem:

(1) Steady-state condition in the period of ΔT
(2) Heat sink radiation to the environment is negligible
(3) Heat enters the heat sink only through the thermoelectric
(4) The base temperature of the heat sink is equal to the temperature of the cold side of the thermoelectric
(5) The contact resistance between the heat sink and thermoelectric is neglected
(6) All the base points of the heat sink have a uniform temperature

4.1. Pipe's energy balance

The schematic view of the pipe's energy balance is presented in Fig. 5. In the present study, the following equations are utilized to calculate the heat transfer in the pipe [38]:

$$\begin{aligned} &E_{in} = E_o \\ &\dot{m}C_p(T_{in} - T_o) = h_{con,p}A_p(T_m - T_p) \end{aligned} \tag{11}$$

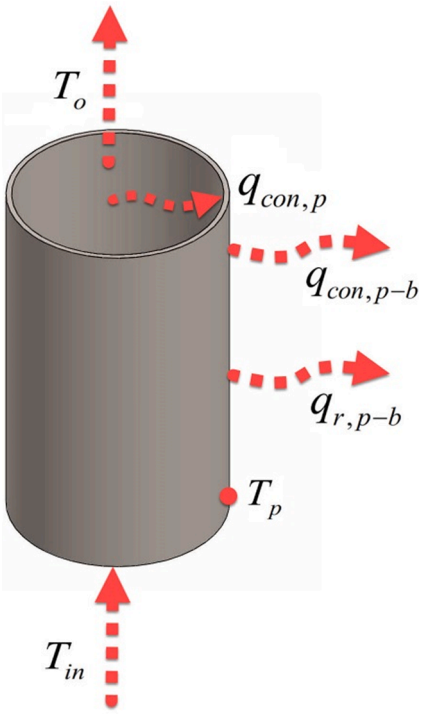

Fig. 5. Energy balance for pipe.

In the above equation, $\dot{m}$, T_{in}, T_o, T_m, T_p, $h_{con,p}$, and A_p are the combusted gas mass flow rate, gas inlet temperature, gas outlet temperature, mean temperature, pipe temperature, convective heat transfer coefficient between gas and pipe, and pipe surface area, respectively.

The convective heat transfer coefficient between gas and pipe is calculated by the following equations [39,40]:

$$h_{con,p} = \frac{Nu_p K}{D} \tag{12}$$

$$Nu_p = 0.59 Ra^{0.25} \tag{13}$$

$$Ra = \frac{g \times \beta \times \Delta T \times D^3 \times Pr}{\nu^2} \tag{14}$$

In the above equations, K, ν, D, and ΔT are the gas thermal conductivity, gas kinematic viscosity, pipe diameter, and temperature difference between gas and pipe surface, respectively. The energy balance equation can be written as follows:

$$q_{con,p} = q_{con,p-b} + q_{r,p-b} \tag{15}$$

where $q_{con,p}$, $q_{con,p-b}$, and $q_{r,p-b}$ represent the input convective heat transfer from combusted gas to the pipe, convective, and radiative heat transfer from pipe to the hollow box, respectively [41,42].

$$q_{con,p} = h_{con,p} A_p (T_m - T_p) \tag{16}$$

$$q_{con,p-b} = h_{con,p-b} A_p (T_p - T_h) \tag{17}$$

$$\begin{aligned} q_{r,p-b} &= h_{r,p-b} A_p (T_p - T_h) \\ h_{r,p-b} &= \sigma F (T_p^2 + T_h^2)(T_p + T_h) \end{aligned} \tag{18}$$

$$T_m = \frac{T_{in} + T_o}{2} \tag{19}$$

Substituting the above Eqs. (16)–(19) in Eq. (15):

$$h_{con,p}(T_m - T_p) = h_{t,p-b}(T_p - T_h) \tag{20}$$

$$h_{t,p-b} = h_{con,p-b} + h_{r,p-b} \tag{21}$$

In the above equation, $h_{t,p-b}$ is the total heat transfer coefficient between the pipe and the hollow box. Through simplifying Eq. (20), the average temperature of combusted gas can be written as follows:

$$T_m = \frac{h_{t,p-b}(T_p - T_h) + h_{con,p} T_p}{h_{con,p}} \tag{22}$$

4.2. Energy balance for the hollow box

Fig. 6 demonstrates a schematic view of the energy balance for the hollow box. In the present work, to calculate the heat transfer equation in the box, the following equations are applied:

$$q_{con,p-b} + q_{r,p-b} = 4 \times q_h \tag{23}$$

where $q_{con,p-b}$, $q_{r,p-b}$, and q_h are convective heat transfer between the pipe and the hollow box, radiative heat transfer from the pipe to the hollow box, and input heat transfer from the box to each thermoelectric module, respectively.

$$q_{con,p-b} = h_{con,p-b} . A_p (T_p - T_h) \tag{17}$$

$$q_{r,p-b} = h_{r,p-b} . A_p (T_p - T_h) \tag{18}$$

$$h_{t,p-b} = h_{r,p-b} + h_{con,p-b} \tag{21}$$

Substituting the above equations in Eq. (23), the temperature of the pipe is expressed as follows:

$$h_{t,p-b} A_p (T_p - T_h) = 4 \times q_h \tag{24}$$

$$T_p = \frac{4 \times q_h + h_{t,p-b} A_p T_h}{h_{t,p-b} A_p} \tag{25}$$

4.3. The thermoelectric module's energy balance

The schematic view of the thermoelectric module's energy balance is depicted in Fig. 7. By considering the steady-state condition, it is deduced that the summation of the generated power and output heat from thermoelectric is equivalent to the thermoelectric module's input heat. In the current study, the contact resistance between the heat sink and thermoelectric is neglected. Therefore, the temperature of the cold side of the thermoelectric and the base temperature of the heat sink are assumed to be equal to T_c. It must also be noted that the transferred heat to the heat sinks only occurs from the thermoelectric modules.

Input and output heat transfer through thermoelectric are as follows [17]:

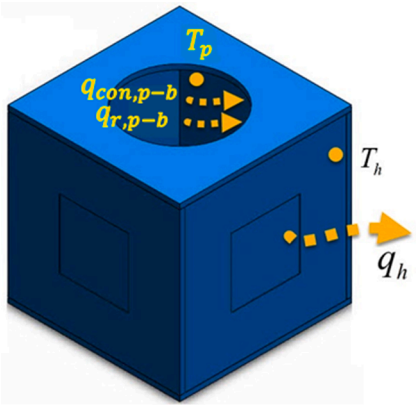

Fig. 6. The hollow box's energy balance.

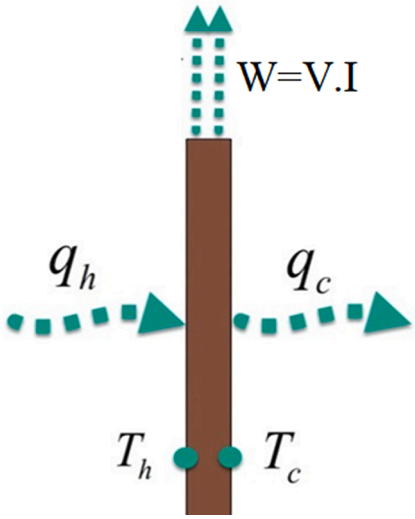

Fig. 7. The thermoelectric module's energy balance.

$$q_h = \alpha_m I T_h - 0.5\rho_m I^2 + \gamma_m \Delta T \tag{26}$$

$$q_c = \alpha_m I T_c + 0.5\rho_m I^2 + \gamma_m \Delta T \tag{27}$$

$$\Delta T = (T_h - T_c) \tag{28}$$

As written below, the generated electrical voltage in thermoelectric is expressed by [20]:

$$V = \alpha_m \Delta T - I\rho_m \tag{29}$$

In a closed circuit, the value of the generated power can be considered as [43]:

$$W = q_h - q_c \tag{30}$$

$$W = VI = \alpha_m I \Delta T - I^2 \rho_m \tag{31}$$

Substituting Eq. (26) and Eq. (28) in Eq. (25), the hot side temperature of the thermoelectric module can be calculated using the following equation:

$$T_h = \frac{h_{t,p-b}A_p T_p + 4\gamma_m T_c + 2\rho_m I^2}{4\alpha_m I + 4\gamma_m + h_{t,p-b}A_p} \tag{32}$$

4.4. Energy balance for the heat sink

The schematic view of the heat sink's energy balance is shown in Fig. 8. Considering that the energy output from the thermoelectric, q_c, and the energy input to the heat sink are equal, the energy balance for the heat sink is written as follows:

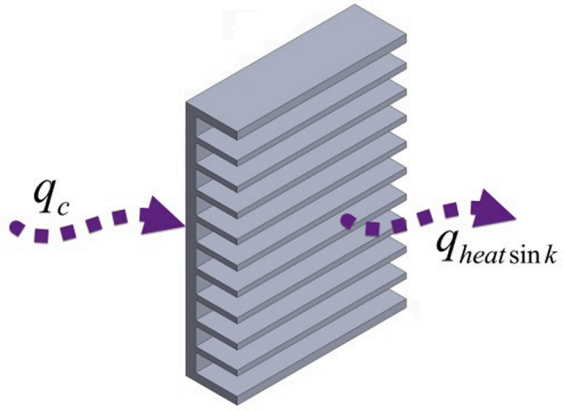

Fig. 8. Energy balance for heat sink.

$$q_{heatsink} = q_c = \frac{T_c - T_a}{R_{heatsink}} \tag{33}$$

Substituting Eq. (27) in the equation above:

$$\alpha_m I T_c + 0.5\rho_m I^2 + \gamma_m \Delta T = \frac{T_c - T_a}{R_{heatsink}} \tag{34}$$

In other words:

$$T_c = \frac{T_a + 0.5\rho_m I^2 R_{heatsink} + \gamma_m T_h R_{heatsink}}{1 + \gamma_m R_{heatsink} - \alpha_m I R_{heatsink}} \tag{35}$$

4.5. Evaluation of the thermoelectric performance

By applying the equations above, the performance of the thermoelectric generator can be evaluated using the following equations:

$$T_m = \frac{T_{in} + T_o}{2} \tag{19}$$

$$T_m = \frac{h_{t,p-b}(T_p - T_h) + h_{con,p}T_p}{h_{con,p}} \tag{22}$$

$$T_p = \frac{4 \times q_h + h_{t,p-b}A_p T_h}{h_{t,p-b}A_p} \tag{25}$$

$$q_h = \alpha_m I T_h - 0.5\rho_m I^2 + \gamma_m \Delta T \tag{26}$$

$$V = \alpha_m \Delta T - I\rho_m \tag{29}$$

$$W = q_h - q_c \tag{30}$$

$$W = VI = \alpha_m I \Delta T - I^2 \rho_m \tag{31}$$

$$T_h = \frac{h_{t,p-b}A_p T_p + 4\gamma_m T_c + 2\rho_m I^2}{4\alpha_m I + 4\gamma_m + h_{t,p-b}A_p} \tag{32}$$

$$T_c = \frac{T_a + 0.5\rho_m I^2 R_{heatsink} + \gamma_m T_h R_{heatsink}}{1 + \gamma_m R_{heatsink} - \alpha_m I R_{heatsink}} \tag{35}$$

As shown in the above equations, there are nine nonlinear equations with nine unknown parameters (T_o, T_m, T_p, T_h, T_c, q_h, V, I, and W). Comprising the values of geometric parameters, gas inlet temperature, ambient temperature, thermoelectric characteristics, heat transfer coefficients, heat sink resistance, and the above equations, we can calculate the unknown parameters using nonlinear algebraic solvers. Note that the heat transfer coefficients between the pipe, box, thermoelectric, and environment depend on the physical and thermal properties of the air, the flow regimes inside the box and the pipe, and the inlet temperature of the combusted gas.

5. Results and discussion

In the previous sections, the experimental method and the mathematical modeling of the proposed system were presented. In this section, the results of this study are discussed.

5.1. Calculations of the generated voltage

This study aimed to express the generated electrical voltage as a function of inlet temperature and ambient temperature through experimental and mathematical procedures. Initially, in this section, via two methods (mathematical modeling and Buckingham Pi theorem) and experimental results, several equations are obtained to estimate the output voltage in terms of air temperature and operating parameters of the proposed system. Following the use of the obtained equations, the

performance of the device under different conditions will be estimated.

5.1.1. Calculation of generated voltage using mathematical modeling

According to Eq. (29), the thermoelectric's generated voltage is calculated as follows:

$$V = \alpha_m \Delta T - I\rho_m = \alpha_m (T_h - T_c) - I\rho_m \tag{29}$$

Based on the above equation, the hot side temperature of the thermoelectric module is expressed as follows:

$$T_h = V\alpha_m^{-1} + \frac{I\rho_m}{\alpha_m} + T_c \tag{36}$$

Combining Eqs. (35) and (36):

$$T_c = (1 - A_0 V)^{-1}\left(T_a + A_1 V^2 + A_2 V\right) \tag{37}$$

where

$$\begin{aligned} A_0 &= \alpha_m R_{heatsink} R_{system}^{-1} \\ A_1 &= 0.5\rho_m R_{heatsink} R_{system}^{-2} \\ A_2 &= \gamma_m R_{heatsink} \alpha_m^{-1} + \gamma_m R_{heatsink} \rho_m \alpha_m^{-1} R_{system}^{-1} \end{aligned} \tag{38}$$

The hot side temperature of the thermoelectric module can be correlated by combining Eqs. (11), (21), (25), and (26):

$$T_h = (B_1 + B_2 V)^{-1}\left(B_0 T_{in} - B_3 T_c - B_4 V^2\right) \tag{39}$$

Where,

$$\begin{aligned} B_0 &= 2\dot{m}C_p h_{con,p} \\ B_1 &= 8\gamma_m \dot{m} C_p A_p^{-1} + 2\dot{m}C_p h_{con,p} + 4\gamma_m h_{con,p} + 8\gamma_m \dot{m} C_p h_{con,p} A_p^{-1} h_{t,p-b}^{-1} \\ B_2 &= 8\alpha_m \dot{m} C_p A_p^{-1} R_{system}^{-1} + 4\alpha_m h_{con,p} R_{system}^{-1} + 8\alpha_m \dot{m} C_p h_{con,p} h_{t,p-b}^{-1} A_p^{-1} R_{system}^{-1} \\ B_3 &= -4\gamma_m h_{con,p} - 8\gamma_m \dot{m} C_p A_p^{-1} - 8\gamma_m \dot{m} C_p h_{con,p} A_p^{-1} h_{t,p-b}^{-1} \\ B_4 &= -2\rho_m h_{con,p} R_{system}^{-2} - 4\rho_m \dot{m} C_p A_p^{-1} R_{system}^{-2} - 4\rho_m \dot{m} C_p h_{con,p} h_{t,p-b}^{-1} A_p^{-1} R_{system}^{-2} \end{aligned} \tag{40}$$

The generated electrical voltage as a function of inlet temperature and ambient temperature can be correlated with Eqs. (29), (37), and (39):

$$\begin{aligned} D_0 V = {} & D_1 V^2 + D_2 V^3 + D_3 V^4 + D_4 T_{in} + D_5 T_{in} V + D_6 T_a V + D_7 T_a + D_8 T_{in} V^2 \\ & + D_9 T_a V^2 \end{aligned} \tag{41}$$

where

$$\begin{aligned} D_0 &= B_1 + B_1 R_{system}^{-1}\rho_m + \alpha_m B_1 A_2 + \alpha_m B_3 A_2 \\ D_1 &= -\alpha_m B_3 A_1 + \alpha_m B_3 A_0 A_2 + B_1 R_{system}^{-1}\rho_m A_0 + 2B_1 A_0 + B_1 R_{system}^{-1}\rho_m A_0 \\ & -B_2 - B_2 R_{system}^{-1}\rho_m - \alpha_m B_4 - \alpha_m A_1 B_1 + \alpha_m B_1 A_2 A_0 - \alpha_m A_2 B_2 \\ D_2 &= \alpha_m B_3 A_0 A_1 - B_1 A_0^2 - B_1 R_{system}^{-1}\rho_m A_0^2 + B_2 R_{system}^{-1}\rho_m A_0 + 2B_2 A_0 \\ & + B_2 R_{system}^{-1}\rho_m A_0 + \alpha_m B_4 A_0 + \alpha_m B_4 A_0 + \alpha_m A_1 B_1 A_0 + \alpha_m A_2 B_2 A_0 - \alpha_m A_1 B_2 \\ D_3 &= -B_2 A_0^2 - B_2 R_{system}^{-1}\rho_m A_0^2 - \alpha_m B_4 A_0^2 + \alpha_m A_1 B_2 A_0 \\ D_4 &= \alpha_m B_0 \\ D_5 &= -2\alpha_m B_0 A_0 \\ D_6 &= \alpha_m B_1 A_0 - \alpha_m B_2 + \alpha_m B_3 A_0 \\ D_7 &= -\alpha_m B_3 - \alpha_m B_1 \\ D_8 &= \alpha_m B_0 A_0^2 \\ D_9 &= \alpha_m B_2 A_0 \end{aligned} \tag{42}$$

It is deduced from Eq. (41) that the generated voltage is a nonlinear function according to the inlet temperature, thermoelectric properties, ambient temperature, radiative and convective heat transfer coefficients, and heat sink resistance. Furthermore, if the changes of D_6, D_5, D_4, D_3, D_2, and D_1 with respect to ambient conditions and temperature are negligible, the voltage generated could be considered as a nonlinear function of inlet temperature and ambient temperature.

5.1.2. Estimation of the generated voltage with Buckingham Pi theorem

The dimensional analysis leads to the elimination of complexity and the reduction of the number of experimental variables affecting a certain physical phenomenon. If a phenomenon depends on n variables with k dimensions, dimensional analysis reduces the number of variables to $n-k$ dimensionless variables depending on the complexity of the problem. Although the goal of dimensional analysis is to decrease the number of variables and group them dimensionless, it also has many advantages, such as saving time and money and helping in designing an experiment or theory. In addition, the most important advantage of this method is that with the help of similarity rules resulting from the dimensional analysis, the data related to a small and inexpensive model can be converted into the design data of a real sample [44].

The previous section revealed that the generated voltage is a function of various parameters, such as dimensions, thermoelectric properties, heat sink resistance, input gas stream temperature, and ambient temperature.

$$V = f(T_a, T_{in} - T_a, D_h, R_{heatsink}, D, \alpha_m, \gamma_m, \rho_m) \tag{43}$$

Table 4 represents the main dimensions of the considered parameters.

Via Buckingham Pi theorem, non-dimensionless parameters can be defined as follows [44]:

$$\begin{aligned} \pi_1 &= \frac{T_{in} - T_a}{T_a} \\ \pi_2 &= \frac{D}{D_h} \\ \pi_3 &= \gamma_m R_{heatsink} \\ \pi_4 &= T_a^{-0.5}\gamma_m^{-0.5}\rho_m^{-0.5} V \\ \pi_5 &= T_a^{0.5}\gamma_m^{-0.5}\rho_m^{-0.5}\alpha_m = \sqrt{ZT_a} \end{aligned} \tag{45}$$

As a result, according to these relations and that π_4 is a function of π_1, π_2, $\pi_3$andπ_5:

$$\begin{aligned} \pi_4 &= f(\pi_1, \pi_2, \pi_3, \pi_5) \\ T_a^{-0.5}\gamma_m^{-0.5}\rho_m^{-0.5} V &= f\left\{\frac{T_{in} - T_a}{T_a}, \frac{D}{D_h}, \gamma_m R_{heatsink}, T_a^{0.5}\gamma_m^{-0.5}\rho_m^{-0.5}\alpha_m\right\} \end{aligned} \tag{46}$$

The function $f(\pi_1, \pi_2, \pi_3, \pi_5)$ is obtained based on the experimental or modeling results employing a curve fitting method (generally using multivariable regression method). Through this function, the amount of generated voltage can be obtained in different conditions. The advantage of using the Buckingham Pi theorem is that the function is dimensionless. Thus, it can be applied in any device with similar geometric and dynamic compared to the existing system (similarity between model and prototype).

Table 4
Main dimensions of parameters.

Parameters	Symbol	Unit	Dimensions
Generated voltage	V	V	$ML^2T^{-3}A^1$
Ambient temperature	T_a	K	θ
Input and ambient temperatures	$T_{in} - T_a$	K	θ
Hollow box hydraulic diameter	D_h	m	L
Heatsink resistance	$R_{heatsink}$	Ω	$\theta T^3 M^{-1} L^{-2}$
Pipe diameter	D	m	L
Seebeck coefficient	α_m	$m^2.s^{-1}$	$ML^2T^{-3}A^{-1}\theta^{-1}$
Thermal conductivity	γ_m	$W.K^{-1}$	$ML^2T^{-3}\theta^{-1}$
Electrical resistance	ρ_m	Ω	$ML^2T^{-3}A^{-2}$

5.2. Experimental results

Experiments were performed on October 3, 2020, in a room with a controlled environment and ambient temperature 22° C. The values of electrical current and output voltage, thermoelectric hot and cold side temperatures, and pipe surface's temperature have been measured in different time intervals.

Fig. 9 represents the variations of the electrical voltage and current during the experiment for each thermoelectric module. As shown in this figure, once the experiment has started, the electrical voltage and current rapidly increased. After 40 min, these values were approximately being constant about 195 mV and 44 mA, respectively.

Fig. 10 shows the variations of the generated voltage and temperature differences between the two sides of the thermoelectric modules during the experiment. As shown in this figure, the temperature difference increases during the experiment and stabilizes (between 43 and 45 K) after 40 min. Moreover, as the temperature difference increases, the output voltage rises.

Fig. 11 presents the variations of the temperature at the tube inlet, the tube surface, and the hot and cold sides of the thermoelectric modules during the experiment. The results indicate that the surface temperature of the tube and the hot and cold temperature of the thermoelectric increase over time. These changes are stabilized after 40 min. Besides, the surface temperature of the tube deviates 6° C from the temperature of the hot side of the thermoelectric, and the temperature difference of the two sides of the thermoelectric is estimated as 16° C.

5.3. Convection heat transfer inside the hollow box

Eq. (15) implies that in order to derive the energy balance inside the hollow box, the convective heat transfer coefficient needs to be estimated between the pipe and the outer surface of the box. Herein, the experimental results were applied to calculate the Nusselt number and convective heat transfer coefficient inside the hollow box. For the hollow box, with applying experimental data and multi-variable linear regression method, the following equations are appropriated:

$$Nu_b = 2.7867 Ra^{0.6986}$$

$$h_{con,p-b} = \frac{Nu_b K}{D_h} \qquad Error_{max} = -6.8\%$$

$$D_h = \frac{4A_b}{P_b} \qquad R^2 = 0.92,$$

The Nusselt number is obtained according to the above equations and experimental data shown in Fig. 12. There is a maximum error of 6.8% in the estimation of the Nusselt number which implies the accuracy of Eq. (47).

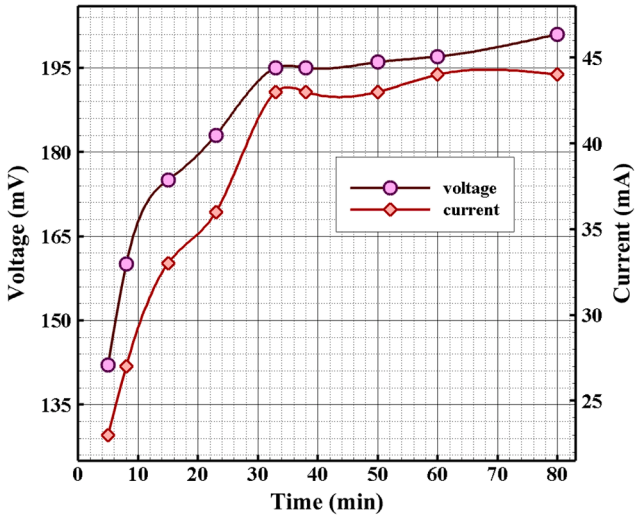

Fig. 9. Variations of voltage and current during the experiment for each thermoelectric.

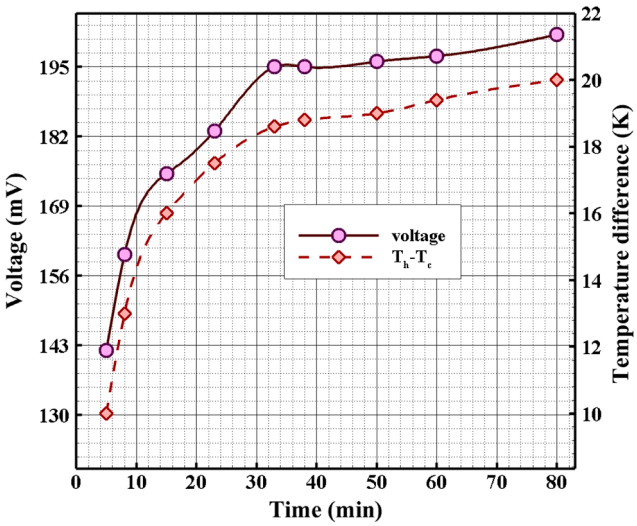

Fig. 10. Variations of the temperature difference between the two sides of thermoelectric during the experiment.

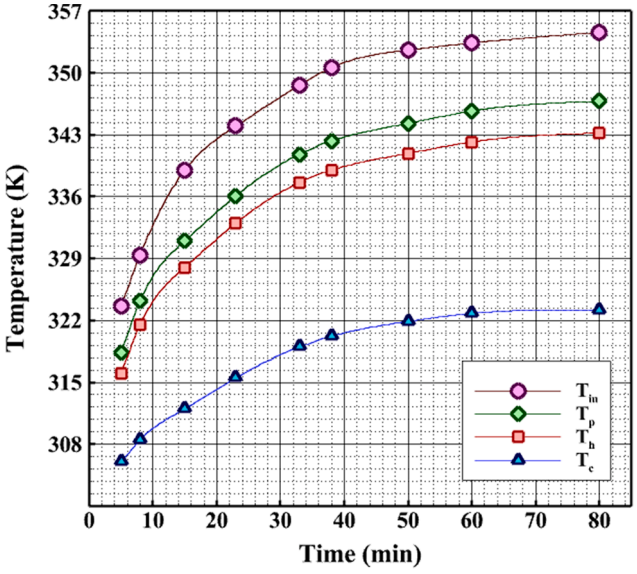

Fig. 11. Variations of temperature during the experiment.

5.4. Proposing several models to predict the generated voltage

The objective of this work is to present a model for predicting the generated voltage. As described in the previous sections, in this study, a device was built, which generated the required electrical voltage with the cathodic protection system from the heat output of the combustion gases. According to Eq. (41), the generated voltage is a function of ambient air temperature and hot air temperature entering the device. In this section, three methods for obtaining this function are presented, and three mathematical models are developed. With these models, the performance of the system can be estimated under different environmental and thermal conditions, without solving the set of nonlinear equations presented in the fourth section or without the need to perform several experiments in various environmental conditions. To obtain the three mathematical models, a computer code is developed to solve the

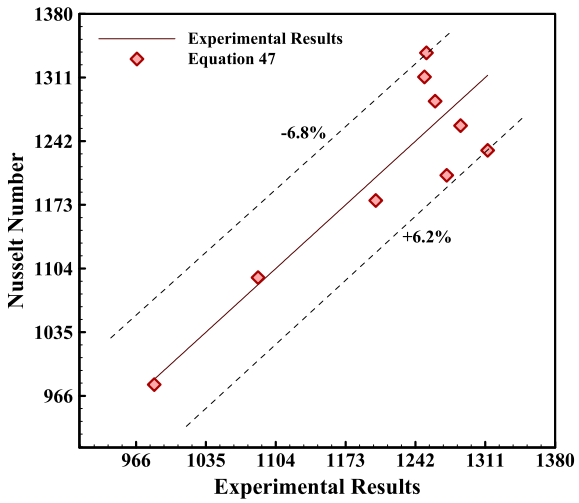

Fig. 12. Comparison between experimental data and Eq. (47) in the estimation of Nusselt number inside the hollow box.

equations presented in the fourth section. Several equations are then proposed for the estimation of the generated voltage by use of multi-variable nonlinear regression method and the results of the computer solver.

5.4.1. Developing a computer code to solve the mathematical modeling equations

Table 5 demonstrates various conditions used as the input data for the computer code. In this table, D_h, D, A_p, α_m,ρ_m, and γ_m are the characteristics of the device, T_{in}, T_p, and T_a are the pipe inlet temperature, the pipe surface temperature and ambient temperature, respectively. $R_{Heatsink}$ was also calculated by the experimental results and Eqs. (23), (26), (27), and (33). Fig. 13 shows a flowchart diagram applied to develop the computer code.

The data of the experiments and developed computer code was compared and revealed in Table 6. Based on the results, there is a 0.75% maximum error in predicting the generated voltage and a 0.77% maximum error in predicting the temperature difference between the two sides of the thermoelectric modules.

5.4.2. First model: Linear curve fitting

According to Eq. (41), the generated voltage can be nonlinearly calculated with the input combusted gas temperature and the ambient temperature within the specified range. Considering the results of mathematical modeling, calculated by the code, and multi-variable linear regression method, the generated voltage is obtained through the following equation:

$$R^2 = 0.99, \quad Error_{max} = 1.22\%, \quad 290 \leqslant T_a \leqslant 313 \quad 320 \leqslant T_{in} \leqslant 350 \tag{48}$$

where V, T_{in}, and T_a are expressed in mV, K, respectively. The results of the experimental data and the above equation have been compared in Fig. 14. The results implied that there is a 1.22% maximum error in the prediction of the generated voltage using Eq. (48). The most important causes of error in this model are considering simplifying assumptions, such as: the neglect of radiative heat transfer, utilizing one-dimensional heat transfer model, and the presence of heat loss in the device. On the other hand, the presence of computational errors, such as round-off errors and truncation errors in nonlinear equation solving algorithm are another cause of errors. However, this equation is in accordance with the experiment results to estimate the generated electrical voltage. This method requires applying nonlinear equation solving techniques, hence, its application is complex, time-consuming, and quite challenging.

5.4.3. Second model: Exponential curve fitting

Solving the nonlinear equation of the previously proposed model is complex, therefore, a new simpler model is proposed, which does not require such a difficult process. Considering the results of mathematical modeling, calculated by the code, and multi-variable linear regression method, the generated voltage can be obtained through the following equation:

$$V = T_{in}^{5.2} \times T_a^{-5.62} \quad R^2 = 0.98, \quad Error_{max} = 9.11\%, \quad 290 \leqslant T_a \leqslant 313 \quad 320 \leqslant T_{in} \leqslant 350 \tag{49}$$

where V, T_{in}, and T_{air} are expressed in mV and K, respectively. Experimental results and the equation above have are compared in Fig. 15. They revealed a maximum error of 9.11% in the prediction of generated voltage. The most important causes of error in this model (the same as previous model) are considering simplifying assumptions, such as the neglect of radiative heat transfer, utilizing one-dimensional heat transfer model, and the presence of heat loss in the device. On the other hand, the presence of computational errors, such as round-off errors and truncation errors in nonlinear equation solving algorithm are other causes of errors. In addition to the errors above, there is an additional error due to the use of multivariable regression method.

5.4.4. Third model: Buckingham Pi theorem

The system performance can be estimated under different geometric,

$$V = 7.96 \times V^2 - 15.95 \times V^3 + 23.05 \times V^4 - 0.00002 \times T_{in} + 0.0001 \times T_{in}V + 0.002 \times T_aV + 0.00006 \times T_a + 0.00003 \times T_{in}V^2 - 0.014 \times T_aV^2$$

Table 5
Values of different parameters for the various test steps used in the computer code.

Time (min)	Case	$R_{Heatsink}(\Omega)$	$T_p(K)$	$D_h(m)$	$D(m)$	$\alpha_m(m^2.s^{-1})$	$\rho_m(\Omega)$	$\gamma_m(W.K^{-1})$	$A_p(m)$	$T_a(K)$	$T_{in}(K)$
5	**1**	0.583	318.3	0.03	0.06	0.01926	2.2	0.8436	0.01884	301	323.6
8	**2**	0.675	324.2	0.03	0.06	0.01687	2.2	0.8436	0.01884	301	329.4
15	**3**	0.805	331	0.03	0.06	0.01547	2.2	0.8436	0.01884	301	339
23	**4**	0.970	336.1	0.03	0.06	0.01498	2.2	0.8436	0.01884	301	344
33	**5**	1.132	340.8	0.03	0.06	0.01557	2.2	0.8436	0.01884	301	348.6
38	**6**	1.194	342.3	0.03	0.06	0.0154	2.2	0.8436	0.01884	301	350.6
50	**7**	1.287	344.3	0.03	0.06	0.01529	2.2	0.8436	0.01884	301	352.6
60	**8**	1.314	345.7	0.03	0.06	0.01514	2.2	0.8436	0.01884	301	353.4
80	**9**	1.299	346.8	0.03	0.06	0.01489	2.2	0.8436	0.01884	301	354.6

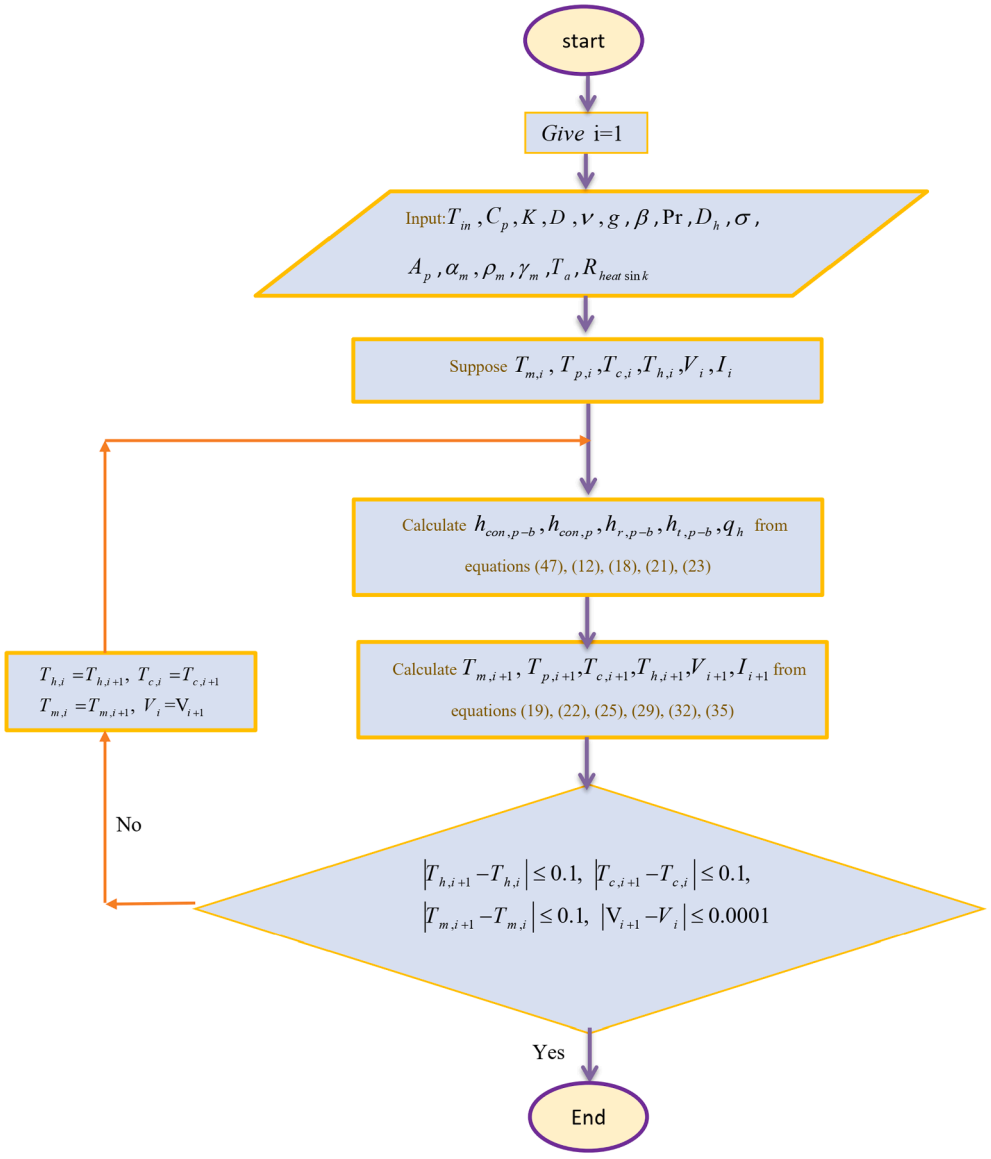

Fig. 13. Flowchart of the developed computer code used to solve mathematical modeling nonlinear equations.

Table 6
Comparison between the code output data and the experimental data.

Case		$T_c(K)$	$T_h(K)$	$\Delta T(K)$	ErrorT	Voltage mV	Error voltage
1	Experimental results	306	316	10	0%	0.1420	
	Computer code results	305.9	315.9	10		0.1425	−0.35%
2	Experimental results	308.5	321.5	13	−0.77%	0.16	−0.75%
	Computer code results	308.5	321.6	13.1		0.1612	
3	Experimental results	312	328	16	0.62%	0.175	
	Computer code results	312	327.9	15.9		0.1758	−0.46%
4	Experimental results	315.5	333	17.5	0.57%	0.183	−0.16%
	Computer code results	315.5	332.9	17.4		0.1833	
5	Experimental results	319	337.6	18.6	−0.54%	0.195	0.46%
	Computer code results	318.8	337.5	18.7		0.1941	
6	Experimental results	320.2	339	18.8	0.53%	0.195	0.15%
	Computer code results	320.1	338.8	18.7		0.1947	
7	Experimental results	321.9	340.9	19	0.53%	0.196	−0.26%
	Computer code results	322	340.9	18.9		0.1965	
8	Experimental results	322.8	342.2	19.4	−0.52%	0.197	−0.36%
	Computer code results	322.8	342.3	19.5		0.1977	
9	Experimental results	323.2	343.2	20	−0.5%	0.201	−0.25%
	Computer code results	323.2	343.3	20.1		0.2015	

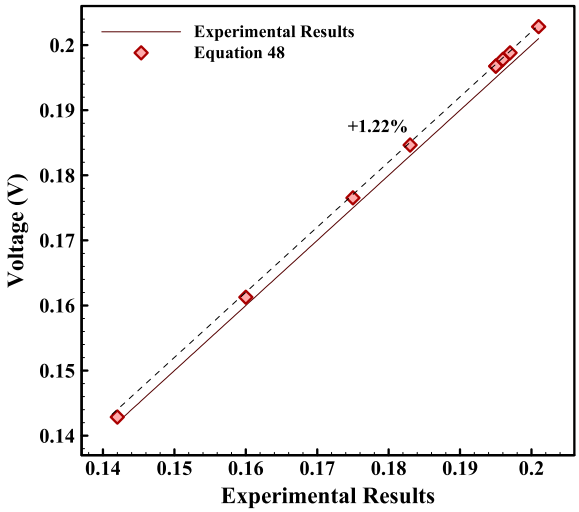

Fig. 14. Comparison between the voltage of Eq. (48) with the experimental data.

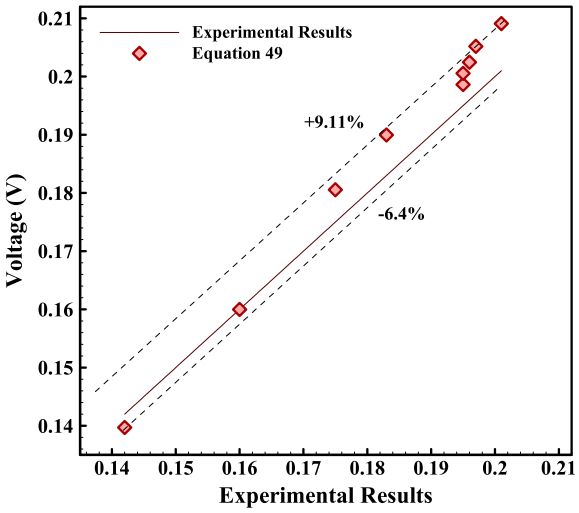

Fig. 15. Comparison between the voltage of Eq. (49) with the experimental data.

environmental conditions through non-dimensioning the equations and parameters affecting the device performance. The forementiond Buckingham Pi theorem is one of the significant and well-known methods of the non-dimensioning of equations, and, with this method, non-dimensionless parameters governing the system can be obtained and discussed.

Eq. (46) implies that π_4 is a function of π_1, π_2, π_3, and π_5. Moreover, the developed computer code was solved, and according to its results and through the use of multi-variable linear regression method and the achieved tip from Eq. (46), the generated voltage can be estimated based on the following equations:

$$\pi_4 = \pi_1^{1.5} \times \pi_2^{0.062} \times \pi_3^{-0.88} \times \pi_5^{1.278}$$

$$T_a^{-0.5} \gamma_m^{-0.5} \rho_m^{-0.5} V = \left(\frac{T_{in} - T_a}{T_a}\right)^{1.5} \times \left(\frac{D}{D_h}\right)^{0.062} \times (\gamma_m R_{heatsink})^{-0.88} \times \left(\sqrt{ZT_a}\right)^{1.278}$$

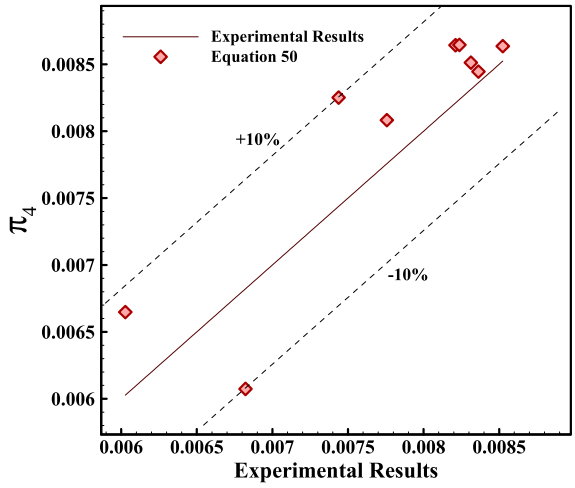

Fig. 16. Comparison between π_4 of Eq. (50) with the experimental data.

$$\begin{aligned} &R^2 = 0.99, && Error_{max} = 10\%, \\ &0.03 \leqslant \frac{T_{in} - T_a}{T_a} \leqslant 0.18 && 0.8571 \leqslant \frac{D}{D_h} \leqslant 3 \\ &0.08436 \leqslant \gamma_m R_{heatsink} \leqslant 1.265 && 0.1767 \leqslant \sqrt{ZT_a} \leqslant 0.2473 \end{aligned} \quad (50)$$

where T_a, T_{in}, γ_m, ρ_m, V, D, D_h, $R_{heatsink}$, and α_m are ambient temperature, inlet temperature, the thermal conductivity of thermoelectric, the electrical resistance of thermoelectric, voltage generated, the diameter of the pipe, the distance between the inner and outer surface of the box, heat sink resistance and Seebeck coefficient, respectively. Fig. 16 represents a comparison between the results of the experimental data and the above equations. The results showed a maximum error of 10% in the prediction of π_4. The most important causes of error are the presence of computational errors, such as round-off errors and the errors associated with the measuring devices.

Fig. 17 represents the effect of changes in π_1, π_3, and π_5 on the dimensionless parameter of π_4. Dimensionless parameters π_1, π_3, and π_5 indicate the ratio of temperature difference to ambient temperature, the effect of heat sink resistance, and the effect of thermoelectric properties (figure of merit), respectively. This figure shows the effect of changing the parameters above on the generated electrical voltage. They also help designers to estimate the produced voltage in any device with the dynamic and geometric similarity to the system utilized in this study. The results show that π_1 has a direct effect on π_4, which means that as the temperature difference (between the inlet gas and the environment) increases, the generated voltage will also rise. However, the effect of π_3 on π_4 is reversed, which means that the output voltage decreases with increasing heat sink resistance. By increasing the heat sink resistance, the temperature difference between the two sides of the thermoelectric module decreases affecting the generated output voltage. Moreover, The results imply that π_5 has a direct effect on π_4. This means that as the figure of merit increases, the generated voltage will also rise.

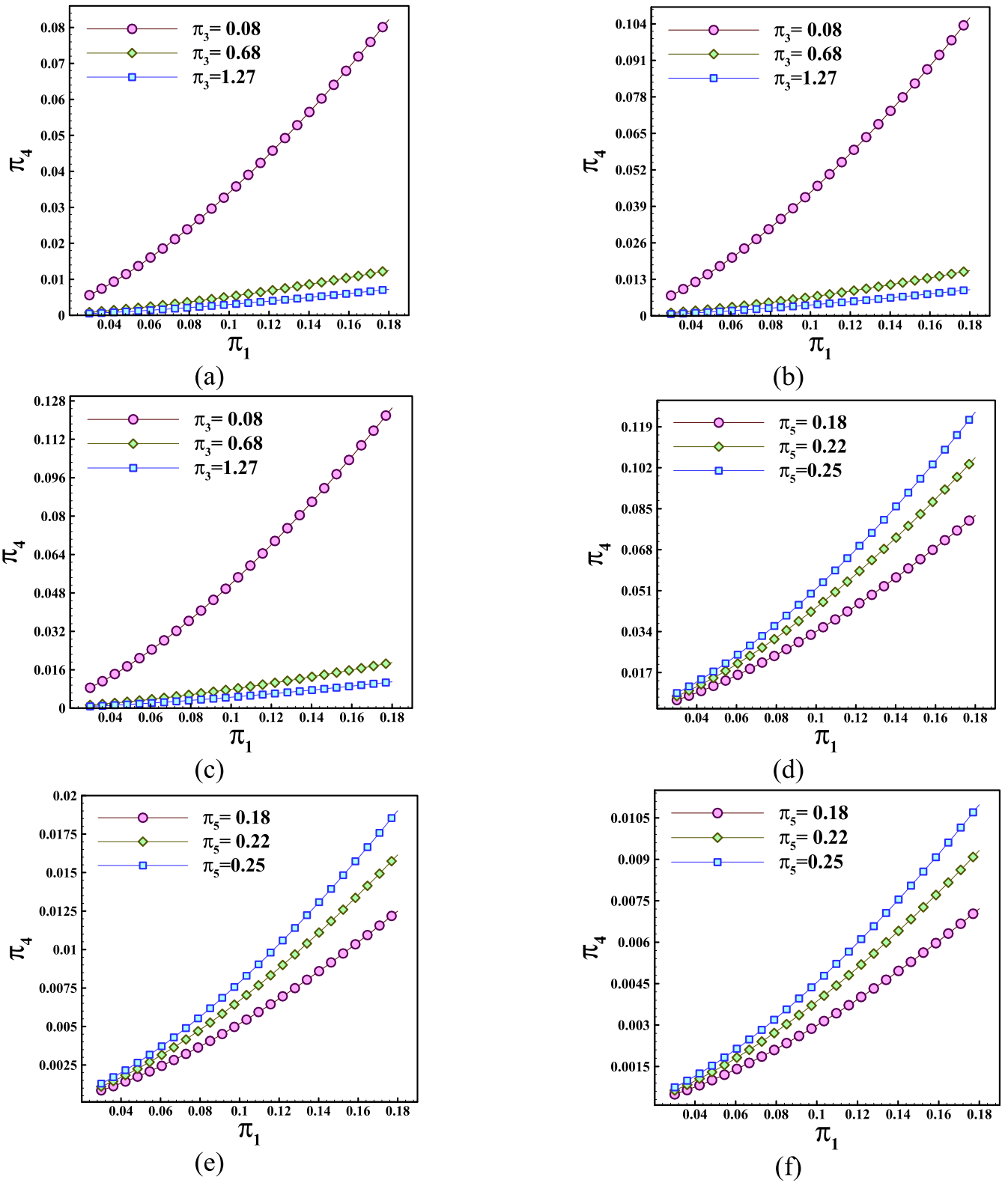

Fig. 17. Variations of π_4 in different values of π_1 when $\pi_2 = 1.977$ and a) $\pi_5 = 0.18$, b) $\pi_5 = 0.22$, c) $\pi_5 = 0.25$, d) $\pi_3 = 0.08$, e) $\pi_3 = 0.68$, f) $\pi_3 = 1.27$.

Table 7
Comparison between the proposing several models.

Models	Generality	Accuracy	Ease of Calculation	Maximum Error
First model		✓		1.22%
Second model			✓	9.11%
Third model	✓			10%

5.4.5. Comparison between the proposed models

In the previous sections, three models were proposed to estimate the generated voltage as a function of ambient and inlet temperature. The first model has higher accuracy than the other models. On the other hand, the second model is much simpler to solve than the others. Although, the third model requires numerical solution and it is more complex than the rest, it can be used in the cathodic protection devices with different types of thermoelectric and heatsinks. Thus, it has more generality. The description above is summarized in Table 7.

6. Conclusion

The objective of the study was to evaluate the performance of an impressed current thermoelectric cathodic protection system. Herein, the experimental and mathematical modeling were employed to derive several models for estimating the device's performance. Moreover, by use of Buckingham Pi theorem, five dimensionless parameters of the system were also achieved. The main results of this study are as follows:

- The generated voltage, electrical current, and temperature difference have been rapidly increased during the experiment up to 201 mV, 44 mA, and 20 K, respectively.
- A new correlation was proposed to calculate the convective heat transfer inside the hollow box with a maximum error of 6.8%.
- A computer code was developed based on the mathematical modeling for the proposed impressed current cathodic protection system with the maximum error of 0.57% in the estimation of the generated voltage.
- The generated voltage is defined as a linear function of the dimensions, thermoelectric properties, heatsink resistance, input gas stream temperature, and ambient temperature.
- Through the use of mathematical modeling, three models have been proposed to predict the generated voltage. First model has a higher accuracy; second model comprises the ease of calculation with lower accuracy while the third model has more generality.
- Two correlations were proposed to calculate the generated voltage as a function of ambient and inlet gas temperatures with the maximum error of 1.22% (First model) and 9.11% (Second model), respectively.
- A dimensionless correlation was presented to calculate the generated voltage with the maximum error of 10%. With this model, the generated voltage could be predicted in similar devices with different types of thermoelectric (different figure of merit (Z)), heatsink resistances, pipes diameters and different environmental conditions.
- The results implied that the increase in temperature difference (between the inlet gas and the environment) will result in an increase in the generated voltage indicating a direct effect of the temperature difference on the generated voltage.
- The results also indicate the inverse and direct effects of the heat sink resistance and the figure of merit (Z) on the generated electrical voltage, respectively.

The aim of this study was to open a new path in modeling the application of thermoelectric modules in cathodic protection devices. There is a suggestion for further work on the application of the thermoelectric technology in the impressed current cathodic protection systems:

- The evaluation of the protection effect of the proposed system and the corrosion rate of the protected pipe
- The replacement of renewable energies, such as solar energy instead of combusted gases in the thermoelectric cathodic protection systems and the evaluation of their performance under different conditions.

CRediT authorship contribution statement

Fatemeh Delfani: Investigation, Software, Validation, Resource, Writing - Original Draft, Visualization, Formal analysis, Methodology, Project administration. **Nader Rahbar:** Methodology, Writing - Review & Editing, Supervision, Conceptualization, Investigation. **Cyrus Aghanajafi:** Review & Editing, Supervision. **Ali Heydari:** Writing - Review & Editing, Supervision, Data Curation. **Abdollah KhalesiDoost:** Review & Editing, Supervision.

Declaration of Competing Interest

The authors declare that they have no known competing financial interests or personal relationships that could have appeared to influence the work reported in this paper.

References

[1] Anwar MS, Sujitha B, Vedalakshmi R. Light-weight cementitious conductive anode for impressed current cathodic protection of steel reinforced concrete application. Constr Build Mater 2014;71:167–80.
[2] Wilson K, Jawed M, Ngala V. The selection and use of cathodic protection systems for the repair of reinforced concrete structures. Constr Build Mater 2013;39:19–25.
[3] Pearson S, Patel R. Repair of Concrete in Highway Bridges: A Practical Guide, Transport Research Laboratory Wokingham, UK; 2002.
[4] Tiba C, de Oliveira EM. Utilization of cathodic protection for transmission towers through photovoltaic generation. Renewable Energy 2012;40(1):150–6.
[5] Adetunji OR, Obakhavbaye RA, Ajileye AK, Adesusi OM, Erinle TJ, Ipadeola SO, et al. Cathodic protection of underground mild steel pipes by impressed current using solar cells as rectifier. J Nigerian Acad Eng 2019;2:12–22.
[6] Lilly MT, Ihekwoaba SC, Ogaji SOT, Probert SD. Prolonging the lives of buried crude-oil and natural-gas pipelines by cathodic protection. Appl Energy 2007;84(9):958–70.
[7] El Ghitani H, Shousha AH. Microprocessor-based cathodic protection system using photovoltaic energy. Appl Energy 1995;52(2-3):299–305.
[8] El-Samahy A-S, Anis WR. Microprocessor based control of photovoltiac cathodic protection system. Energy Convers Manage 1997;38(1):21–7.
[9] Laoun B, Niboucha K, Serir L. Cathodic protection of a buried pipeline by solar energy. Revue des Energies Renouvelables 2008;12(1):99–104.
[10] Javadi M, Javidan J, Salimi M. Design an intelligent solar photovoltaic power for cathodic protection system to protect under ground gas pipeline. Int J Tech Phys Probl Eng 2014;6(1):27–33.
[11] Polder RB, Leegwater G, Worm D, Courage W. Service life and life cycle cost modelling of cathodic protection systems for concrete structures. Cem Concr Compos 2014;47:69–74.
[12] Gadala IM, Abdel Wahab M, Alfantazi A. Numerical simulations of soil physicochemistry and aeration influences on the external corrosion and cathodic protection design of buried pipeline steels. Mater Des 2016;97:287–99.
[13] Hameed KW, Yaro AS, Khadom AA. Mathematical model for cathodic protection in a steel-saline water system. J Taibah Univ Sci 2016;10(1):64–9.
[14] Lorenzi S, Pastore T, Bellezze T, Fratesi R. Cathodic protection modelling of a propeller shaft. Corros Sci 2016;108:36–46.
[15] Meng J-H, Wang X-D, Zhang X-X. Transient modeling and dynamic characteristics of thermoelectric cooler. Appl Energy 2013;108:340–8.
[16] Friedensen VP. Space nuclear power: Technology, policy, and risk considerations in human missions to Mars. Acta Astronaut 1998;42(1–8):395–409.
[17] Rahbar N, Asadi A. Solar intensity measurement using a thermoelectric module; experimental study and mathematical modeling. Energy Convers Manage 2016;129:344–53.
[18] Omidi B, Rahbar N, Kargarsharifabad H, Rashidi S. Combination of a solar collector and thermoelectric cooling modules in a humidification–dehumidification desalination system-experimental investigation with energy, exergy, exergoeconomic and environmental analysis. Energy Convers Manage 2020;225:113440.
[19] Shoeibi S, Rahbar N, Esfahlani AA, Kargarsharifabad H. Application of simultaneous thermoelectric cooling and heating to improve the performance of a solar still: An experimental study and exergy analysis. Appl Energy 2020;263:114581.
[20] Hasani M, Rahbar N. Application of thermoelectric cooler as a power generator in waste heat recovery from a PEM fuel cell – An experimental study. Int J Hydrogen Energy 2015;40(43):15040–51.
[21] Vella GJ, Harris LB, Goldsmid HJ. A solar thermoelectric refrigerator. Sol Energy 1976;18(4):355–9.

[22] Yu S, Du Q, Diao H, Shu G, Jiao K. Start-up modes of thermoelectric generator based on vehicle exhaust waste heat recovery. Appl Energy 2015;138:276–90.
[23] Ali G, Wagner J, Moline D, Schweisinger T. Energy harvesting from atmospheric variations – Theory and test. Renew Energy 2015;74:528–35.
[24] Yezhov V, Semicheva N, Pakhomova E, Burtsev A, Brezhnev A, Perepelitsa N. Characterization of Thermoelectric Generators for Cathodic Protection of Pipelines of the City Heating, Energy Management of Municipal Transportation Facilities and Transport, Springer; 2018, pp. 670-678.
[25] Rahman MF. Analisa Penggunaan Thermoelectric Sebagai Sumber Arus Listrik Pada Impressed Current Cathodic Protection (Iccp) Di Pelat Lambung Kapal. Institut Teknologi Sepuluh Nopember Surabaya 2016.
[26] Lishu W, Xinran L, Jiheng S, Xu Z, Shida S. Improvement of cathodic protection of greenhouse buried heat-supply metal pipeline based on thermoelectric cell. Trans Chin Soc Agric Eng 2018;2018:19.
[27] Bergman TL, Incropera FP, Lavine AS, Dewitt DP. Introduction to heat transfer. John Wiley & Sons; 2011.
[28] Yang X, Lu Z, Bai Q, Zhang Q, Jin L, Yan J. Thermal performance of a shell-and-tube latent heat thermal energy storage unit: Role of annular fins. Appl Energy 2017;202:558–70.
[29] Kavian S, Aghanajafi C, Mosleh HJ, Nazari A, Nazari A. Exergy, economic and environmental evaluation of an optimized hybrid photovoltaic-geothermal heat pump system. Appl Energy 2020;276:115469.
[30] Siahmargoi M, Rahbar N, Kargarsharifabad H, Sadati SE, Asadi A. An experimental Study on the performance evaluation and thermodynamic Modeling of a thermoelectric cooler combined with two Heatsinks. Sci Rep 2019;9(1):1–11.
[31] Esfahani JA, Rahbar N, Lavvaf M. Utilization of thermoelectric cooling in a portable active solar still—an experimental study on winter days. Desalination 2011;269(1-3):198–205.
[32] Shoeibi S, Rahbar N, Esfahlani AA, Kargarsharifabad H. Energy matrices, exergoeconomic and enviroeconomic analysis of air-cooled and water-cooled solar still: Experimental investigation and numerical simulation. Renew Energy 2021; 171:227–44.
[33] Shoeibi S, Rahbar N, Esfahlani AA, Kargarsharifabad H. Improving the thermoelectric solar still performance by using nanofluids–Experimental study, thermodynamic modeling and energy matrices analysis. Sustain Energy Technol Assess 2021;47:101339.
[34] Rahbar N, Esfahani JA, Asadi A. An experimental investigation on productivity and performance of a new improved design portable asymmetrical solar still utilizing thermoelectric modules. Energy Convers Manage 2016;118:55–62.
[35] Alipanah F, Rahbar N. CFD simulation and second law analysis of weir-type cascade solar stills with different number and dimensions of steps. Desalin Water Treat 2018;104:15–27.
[36] Rahbar N, Taherian M, Shateri M, Valipour S. Numerical investigation on flow behavior and energy separation in a micro-scale vortex tube. Therm Sci 2015;19 (2):619–30.
[37] Khatami S, Rahbar N. An Analytical study of entropy generation in rectangular natural convective porous fins. Therm Sci Engneering Progress 2019;11:142–9.
[38] Stevens RJ, Weinstein SJ, Koppula KS. Theoretical limits of thermoelectric power generation from exhaust gases. Appl Energy 2014;133:80–8.
[39] Ohk S-M, Chung B-J. Natural convection heat transfer inside an open vertical pipe: influences of length, diameter and Prandtl number. Int J Therm Sci 2017;115: 54–64.
[40] Abbassi H, Aghanajafi C. Evaluation of heat transfer augmentation in a nanofluid-cooled microchannel heat sink. J Fusion Energy 2006;25(3-4):187–96.
[41] Karami A, Yousefi T, Mohebbi S, Aghanajafi C. Prediction of free convection from vertical and inclined rows of horizontal isothermal cylinders using ANFIS. Arabian J Sci Eng 2014;39(5):4201–9.
[42] Aranguren P, Astrain D, Rodríguez A, Martínez A. Experimental investigation of the applicability of a thermoelectric generator to recover waste heat from a combustion chamber. Appl Energy 2015;152:121–30.
[43] Hsu C-T, Huang G-Y, Chu H-S, Yu B, Yao D-J. An effective Seebeck coefficient obtained by experimental results of a thermoelectric generator module. Appl Energy 2011;88(12):5173–9.
[44] Yunus AC. Fluid Mechanics: Fundamentals and Applications (Si Units). Tata McGraw Hill Education Private Limited; 2010.